Lock-in common-mode rejection demodulation: Measurement technique and applications to thermal-wave detection. Experimental

Stefano Paoloni,[a] Lena Nicolaides, and Andreas Mandelis[b]

Photothermal and Optoelectronic Diagnostics Laboratories, Department of Mechanical and Industrial Engineering, University of Toronto, and Materials and Manufacturing Ontario, Toronto M5S 3G8, Canada

A new signal generation methodology based on lock-in amplifier common mode rejection demodulation for materials nondestructive evaluation has been implemented experimentally with thermal waves in a photothermal radiometric apparatus. A procedure to calibrate the experiment is described in order to take into account instrumental time delay phase shifts between the reference and the optical excitation wave form. Some preliminary results obtained on Zr–2.5Nb shot peened samples are presented and compared to those obtained by temporally modulating the pump intensity as a 50% duty cycle square wave. The comparison shows the new measurement methodology to be a very promising technique for nondestructive evaluation and depth profiling applications, featuring high detectivity for low-dynamic-range and poor-signal to noise ratio signals, such as those obtained with thermal-wave diagnostics. © *2000 American Institute of Physics.* [S0034-6748(00)03206-8]

I. INTRODUCTION

A new lock-in common-mode rejection demodulation scheme offering substantial dynamic range enhancement of general signals using lock-in amplifier (LIA) detection has been introduced.[1] In particular, this scheme has been shown to be very promising for high-resolution thermal-wave nondestructive material evaluation (NDE) applications. The method is essentially a real-time differential signal generation technique without the requirement for two excitation sources or two sample geometries. If the sample is irradiated with a periodic optical wave form consisting of two pulses, then the LIA output is basically given by the *difference* of the physical response wave forms produced by each of the two pulses. This fact is of fundamental importance toward the improvement of low-dynamic range techniques, such as thermal-wave NDE, in their ability to detect relatively small signal variations from slightly different materials. In practice, the differential action has the effect of suppressing the signal baseline, which leads to an enhanced detectivity when compared to conventional single-ended techniques. Thus, the instrumental sensitivity is not compromised by the high-level signal baseline and can easily match the level of small signal variations introduced by slightly different materials or by very weak inhomogeneities in a given material.

Another important advantage of the differential action is given by the improvement of the signal-to-noise ratio (SNR) due to the common-mode signal noise rejection. This decreases the noise level substantially enough so as to allow the probing of those weak signal variations which are normally obscured by noise in conventional single-ended techniques.

The modulation wave form that accomplishes the differential LIA action is shown in Fig. 1. Theoretically, we have shown[1] that the LIA in-phase (IP) and quadrature (Q) components are given by a linear combination of two instrumental functions depending on both the optical wave form parameters (τ_1, τ_2, Δ) and the real and imaginary part of the complex photothermal response $S(f)$. By properly selecting the optical wave form $i(t)$ parameters, it is possible to obtain a zero value for either the IP or Q component at *any* modulation frequency f. The presence of these zeroes, which are due to the balancing of energy transport effects produced by the two optical pulses, offers an alternative way for materials inspections. If a sample has different properties, and therefore different photothermal response $S(f)$ from a homogeneous reference sample, then the zero magnitude condition cannot be achieved for the same optical wave form parameters. Despite a more complicated relationship between the LIA response and the photothermal response, this kind of methodology is very promising, especially if one is interested in the detection of minute thermal inhomogeneities.

In this work, some calibration measurements obtained on a homogeneous Zr alloy sample will be presented. These measurements will be further compared with that obtained by irradiating the sample with the conventional 50% duty-cycle square wave, in order to compare their noise characteristics. Finally, some preliminary measurements on Zr–2.5Nb shot peened samples will be presented as a case study of weakly inhomogeneous solids and for comparison with that obtained with the conventional frequency scan.[2]

II. INSTRUMENTATION, MEASUREMENT, AND CALIBRATION PROCEDURES

A simple laser-infrared radiometric photothermal (PTR) embodiment of the common-mode rejection LIA methodology was constructed. A schematic diagram of the experimental setup used to perform the PTR measurements is shown in

---

[a]On leave from INFM-Universita' di Roma ''La Sapienza,'' Dipartimento di Energetica Via Scarpa 16, 00161 Roma, Italy.
[b]Author to whom correspondence should be addressed; electronic mail: mandelis@mie.utoronto.ca
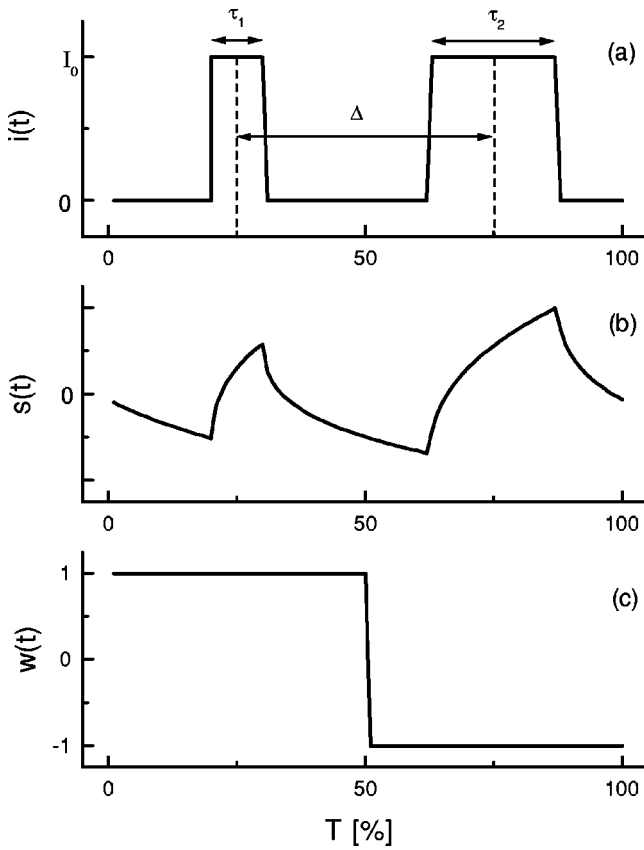
      2445

FIG. 1. (a) Optical excitation pulse train $i(t)$; (b) photothermal repetitive transient signal $s(t)$ due to $i(t)$; (c)lock-in weighting function $w(t)$.

Fig. 2. An Ar ion laser (514 nm) from Coherent, model Innova 100, was used as a 250 mW pump beam with a 2 mm spot size impinging on the sample surface. The beam was intensity modulated by an acousto-optic modulator (AOM), the digital driver of which was connected to a four channel delay digital generator (Stanford Research Model DG535). The digital delay generator allowed the construction of the two-square-pulse wave form used to drive the AOM through the driver. The emitted infrared (IR) radiation from the sample was collected and focused onto the detector using two Ag coated off-axis paraboloidal mirrors. The detector
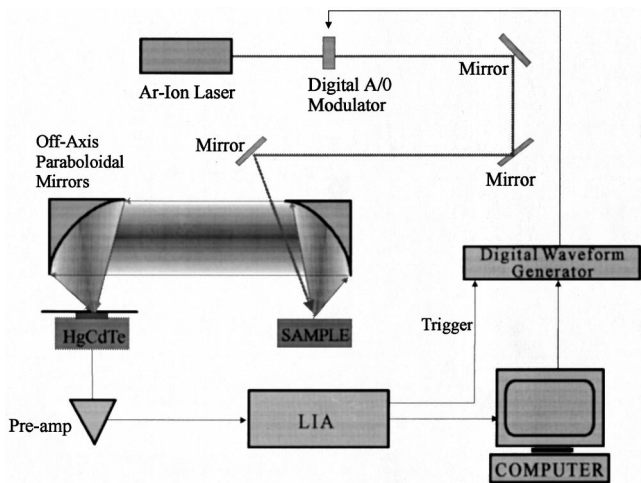

FIG. 2. Block diagram of the experimental infrared radiometric setup.

was a liquid-nitrogen-cooled HgCdTe (EG&G Model J15D12) detector with an active area of 1 mm^2. A Ge window was mounted in front of the detector to block any visible radiation from the pump laser. The PTR signal from the detector was preamplified (EG&G Judson Model PA 350) and fed to an analog LIA (EG&G model 5210), which also provided the external triggering signal for the digital delay generator. A personal computer was used to control the modulation wave form and to store the LIA signal components.

As a first step, several experiments were performed using a crystalline Zr alloy ''reference'' sample. The experiment consisted of recording the PTR signal as a function of the two-pulse separation for different widths of the first pulse while the width of the second pulse remained fixed ($\tau_2/T = 25\%$). The separation scan range was limited by the necessity to avoid the overlapping of the two pulses. In fact, linear conduction heat transfer theory relies on a linear superposition of the effect of each pulse, which further implies that the optical intensity should be two times higher when the pulses are driving the AOM in tandem. This condition is not fulfilled under normal, single-ended working conditions of the modulator. The aim of these measurements was to measure the instrumental time-delay shift that inevitably occurs between the reference and the optical excitation wave form due to the finite risetime of the modulator and the peripheral electronics. In order to fit the data, the theoretical expressions for the IP and Q components of the LIA[1] have been modified by inserting a time delay term d:

$$
\begin{aligned}
Y_{\mathrm{IP}}(f) = -\frac{2I_0}{\pi}\Bigg\{ &\cos\left(\frac{\pi(\Delta+d)}{T}\right)\left[\sin\left(\frac{\pi\tau_1}{T}\right)\right. \\
&+ \sin\left(\frac{\pi\tau_2}{T}\right)\bigg]\mathrm{Re}[S(f)]+\sin\left(\frac{\pi(\Delta+d)}{T}\right) \\
&\times\left[\sin\left(\frac{\pi\tau_1}{T}\right)-\sin\left(\frac{\pi\tau_2}{T}\right)\right]\mathrm{Im}[S(f)]\Bigg\}
\end{aligned}
\tag{1}
$$

and

$$
\begin{aligned}
Y_Q(f) = \frac{2I_0}{\pi}\Bigg\{ &\sin\left(\frac{\pi(\Delta+d)}{T}\right)\left[\sin\left(\frac{\pi\tau_1}{T}\right)\right. \\
&- \sin\left(\frac{\pi\tau_2}{T}\right)\bigg]\mathrm{Re}[S(f)]-\cos\left(\frac{\pi(\Delta+d)}{T}\right) \\
&\times\left[\sin\left(\frac{\pi\tau_1}{T}\right)+\sin\left(\frac{\pi\tau_2}{T}\right)\right]\mathrm{Im}[S(f)]\Bigg\}.
\end{aligned}
\tag{2}
$$

The introduction of the delay term d shifts the crossing points for the IP and Q channels,[1] which, according to Eqs. (1) and (2), must be modified as follows

$$
\begin{aligned}
&\tan\left[\frac{\pi}{T}(\Delta_{0,\mathrm{IP}}+d)\right] \\
&= \left\{\frac{\mathrm{Re}[S(f)]}{\mathrm{Im}[S(f)]}\frac{\sin\left(\frac{\pi\tau_1}{T}\right)+\sin\left(\frac{\pi\tau_2}{T}\right)}{\sin\left(\frac{\pi\tau_2}{T}\right)-\sin\left(\frac{\pi\tau_1}{T}\right)}\right\},
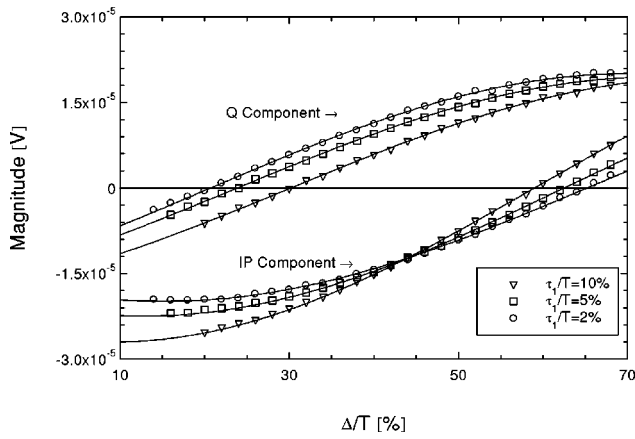\end{aligned}
\tag{3}
$$

FIG. 3. Experimental IP and Q component data obtained on a Zr alloy sample for the τ_1/T values reported in the inset. The modulation frequency was $f = 10$ kHz and $\tau_2/T = 25\%$. The solid lines represent the theoretical fits calculated according to Eqs. (1) and (2) assuming $\text{Re}[S(f)] = -\text{Im}[S(f)]$.
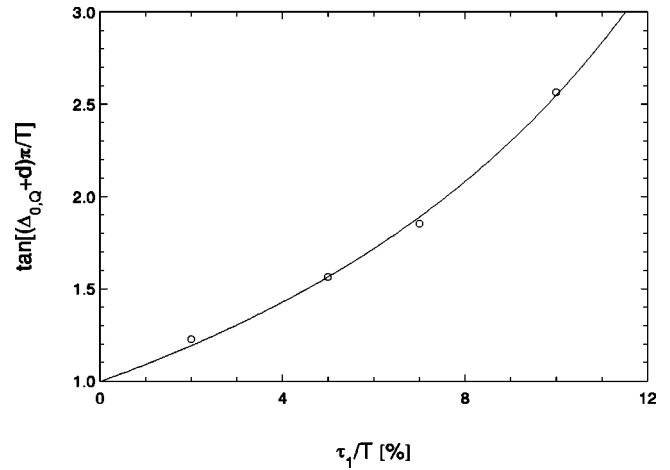
$$\tan\left[\frac{\pi}{T}(\Delta_{0,Q}+d)\right]$$

$$= \left\{\frac{\text{Im}[S(f)]}{\text{Re}[S(f)]}\frac{\sin\left(\frac{\pi\tau_1}{T}\right)+\sin\left(\frac{\pi\tau_2}{T}\right)}{\sin\left(\frac{\pi\tau_1}{T}\right)-\sin\left(\frac{\pi\tau_2}{T}\right)}\right\}. \tag{4}$$

The experimental results have been fitted to the theoretical expressions, Eqs. (1) and (2), by using d as an adjustable parameter (fixed for a given repetition frequency), and assuming $\text{Re}[S(f)] = -\text{Im}[S(f)]$, which is theoretically consistent with the assumption of a homogeneous (reference) sample.[3] It should be noted that, like the single-ended technique, the use of a reference sample here may be confined to calculating the one-point instrumental transfer-function phase shift at the given frequency. Furthermore, the position of the two zero-crossing signal magnitude points (one for the IP and one for the Q channel) can also be labeled as belonging to a homogeneous sample. Nevertheless, the former operation is not essential when only the degree of departure from homogeneity of a test sample is required.

Measurements with the Zr alloy sample have been performed at three modulation frequencies (0.5, 5, and 10 kHz). Typical experimental results are shown together with their theoretical fits in Fig. 3. We wish to point out the excellent agreement between theory and experimental results, which is

FIG. 4. Experimental Q component zero crossing values obtained on the Zr alloy sample with $\tau_1/T = 2\%$, 5%, 7%, and 10%. The modulation frequency is 5 kHz while $\tau_2/T = 25\%$.

indicative of the potential of the technique, in view of the very low signal levels encountered, especially at 10 kHz. This is the result of the efficient noise suppression, in part due to the common-mode rejection by the differential operation performed by the LIA, and in part due to the constant noise bandwidth of the fixed-frequency operation, as discussed in Sec. III of Part I.[1]

In Table I, the instrumental delays obtained for both the IP and Q components are shown for the various modulation frequencies of our experiments. It is noted that for a given frequency the delay values for the Q component are quite independent of τ_1 as they should be, while those for the IP component reveal a greater scatter. We believe that this is due to the fact that the zeroes of the IP component are close to the upper edge of the Δ scan (Fig. 3) and the fitting procedure cannot afford the same quality as that for the Q component. For this reason we will henceforth limit our attention only to the Q component of the signal.

In order to study the influence of the scatter in the delay data on the performance of the experiment, we inserted the average d value in Eq. (2) reported in the last row of Table I, and we again fitted all the data in order to find the $\text{Im}[(S(f)]/\text{Re}[S(f)]$ ratio or, equivalently, the $\Delta_{0,Q}$ zero crossing positions. The $\tan[(\Delta_{0,Q}+d)\pi/T]$ values obtained for the Q component at 5 kHz as a function of τ_1/T are reported in Fig. 4, together with the theoretical interpolation given by Eq. (4) with $\text{Im}[(S(f)]/\text{Re}[S(f)]$ as a parameter. The quality of the fits for the remaining frequencies (0.5 and

TABLE I. Delay term d/T as a function of f and τ_1/T obtained by fitting the IP and Q components of the Zr response to Eqs. (1) and (2) assuming $\text{Re}[S(f)] = -\text{Im}[S(f)]$. τ_2/T was equal to 25%. Last row shows the average d value in each column.

τ_1/T (%)	$f = 500$ Hz		$f = 5$ kHz		$f = 10$ kHz	
	IP	Q	IP	Q	IP	Q
2	2.20	2.36	2.22	2.39	6.98	7.13
5	2.16	2.28	2.02	2.87	5.47	8.09
7	2.11	2.39	2.07	3.11	4.44	8.10
10	1.95	2.05	1.22	2.76	2.88	7.94
avg	2.1	2.3	1.9	2.8	5.0	7.8

TABLE II. $\mathrm{Im}[S(f)]/\mathrm{Re}[S(f)]$ ratio values for the three investigated samples (two shot peened Zr–2.5Nb alloys and the reference Zr sample) obtained by fitting the zero crossing points to Eq. (4).

Sample	$f = 0.5$ kHz	$f = 5$ kHz	$f = 10$ kHz
Zr	−1.01	−0.99	−1.00
C5	−0.928	−0.955	−0.996
N7	−1.12	−0.929	−0.964

10 kHz) was very similar. It is concluded that the *d*-value scatter has a negligible effect on the output response, which results in excellent agreement between the experimental data and the expected theoretical result for Zr ($\mathrm{Im}[S(f)]/\mathrm{Re}[S(f)] = -1$); see first row of Table II. This agreement means that, in general, the instrumental delay can be assumed constant for a given frequency, as long as distortions are not introduced in the optical wave form shape. Moreover it should be noted that this calibration is sample independent. This means that for a given experimental apparatus the delay values remain the same and it is not necessary to repeat the calibration.

In order to evaluate the robustness of this new methodology, the same pulse separation scans have been performed for various pump laser powers. Conventional frequency scans have also been carried out in parallel under the same experimental conditions, in order to compare the relative SNR. In Fig. 5 the *Q* component is reported as a function of pulse separation. As can be seen, even the data corresponding to the lowest power are in agreement with the other sets despite the very low magnitude (less than 2 μV). The varying slopes of the experimental data about the zero crossing point are due to the corresponding $S(f)$ amplitudes.[1] The zero crossing points are coincident for all experimental laser powers, as expected from the same sample, and very good noise rejection is observed.

The corresponding signal phase data, obtained by temporally varying the pump intensity as a 50% duty-cycle square wave, are reported in Fig. 6. The data corresponding to the two highest power values are in agreement, but those obtained at the lowest power are increasingly shifted with
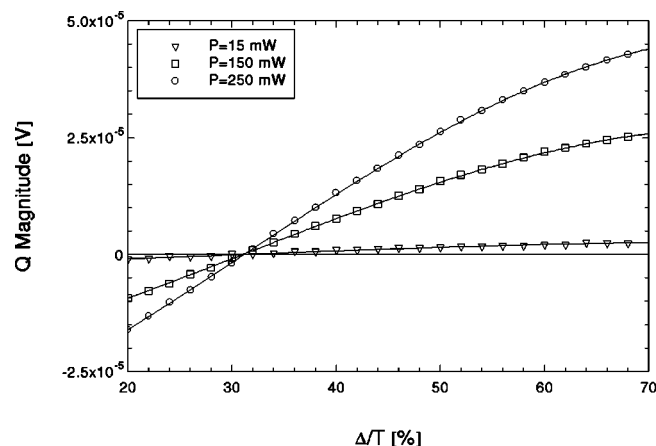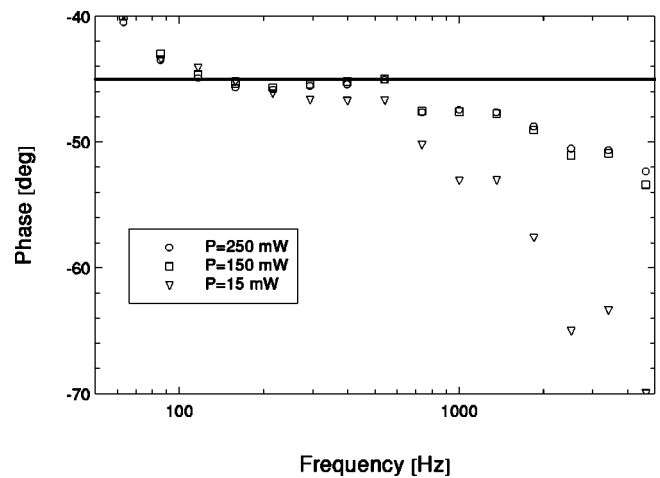

FIG. 6. Conventional frequency-scan phase signals obtained for the pump power values reported in Fig. 5.

increasing modulation frequency. In the frequency range utilized in the pulse-scan measurements ($f = 500$ Hz), the phase shift is approximately $-1.5°$. In order to give a comparison between the two methodologies, Fig. 7 shows a zoom in the vicinity of the zero crossing region of the curves reported in Fig. 5. Here two additional curves are included, showing the theoretical interpolation of the data obtained for $P = 150$ mW, arbitrarily shifted by $\pm 1.5°$ with respect to $\arg[(Sf)] = -45°$ (the semi-infinite photothermal case). It is evident that the spread Δ_2 among the crossing points at all laser powers is much less than the phase-error equivalent spread Δ_1 ($1.5°$ exhibited by the frequency scan). Once again, this confirms the good noise suppression resulting from the lock-in differential action.

III. EXPERIMENTAL RESULTS ON SHOT-PEENED Zr–2.5Nb

After the preliminary tests with the Zr alloy reference and the ensuing calibration procedure, experiments were performed with two Zr–2.5Nb shot-peened samples in order to test the sensitivity of the new instrumental methodology to

FIG. 5. *Q* magnitude pulse-separation scans obtained for $\tau_1/T = 5\%$, $\tau_2/T = 25\%$, $f = 500$ Hz and for the pump laser power values shown in the inset. Continuous lines are theoretical fits to Eq. (4) with $\mathrm{Im}[(S(f)]/\mathrm{Re}[(S(f)]$ as the only adjustable parameter.
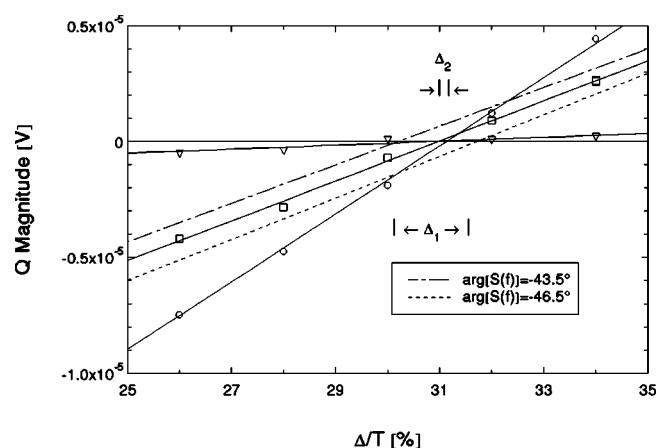

FIG. 7. Zoom of the data reported in Fig. 5 in the vicinity of the zero crossing region. The solid lines are theoretical fits calculated according to Eq. (2). The dotted curves represent the theoretical data obtained for $P = 150$ mW, calculated for $\arg[(S(f)]$ values reported in the inset.
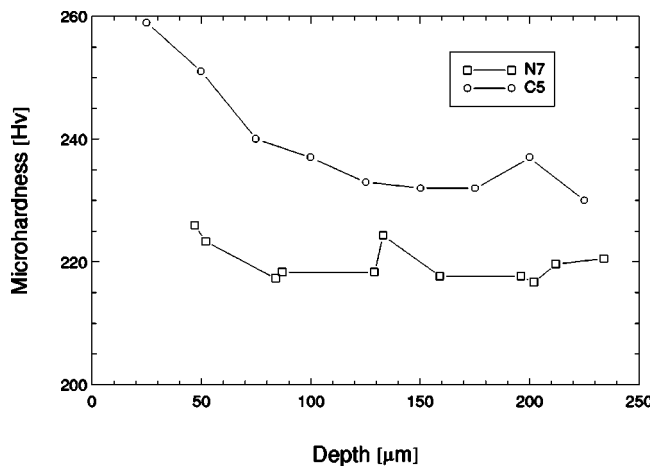
FIG. 8. Microhardness depth profiles for two shot peened Zr–2.5Nb alloy samples. The inset shows Almen intensities. The data corresponding to the N7 sample have been smoothed.

minute thermomechanical inhomogeneities and to compare the results with those obtained by means of the conventional 50% duty-cycle frequency-scan PTR method. Shot peening[4] is employed as an effective mechanical surface improvement method in metallic materials. This method basically consists of bombarding the metal surface with a large number of small spheres of steel, glass, or ceramic, totally covering the surface with indentations. As a result, a thin surface layer (on the order of 100 μm) is plastically deformed. Plastic deformation causes strain hardening, which improves the fatigue life and corrosion resistance of the treated metal surface. In selecting and controlling shot peening parameters to optimize surface improvement, it is very important to monitor the effects caused by the shot peening process. These effects to date are usually evaluated by destructive methods, such as transmission electron microscopy (TEM).

The two examined samples were shot peened at Almen intensities C5 and N7, respectively. The microhardness profiles obtained by Vickers indentation tests are shown in Fig. 8. Sample C5 reveals quite a small variation ($\approx 10\%$) in the hardness value over a depth distance on the order of 100 μm, while sample N7 exhibits an essentially flat hardness profile. Nevertheless, TEM examinations performed on this same sample have indicated that shoot peening at N7 Almen intensity *does affect* the grain structure over a depth lower than 60 μm.[5] The foregoing shot peening process was chosen to test the new technique because its effects on the thermophysical properties of metals are minuscule. For comparison, photothermal depth profilometry of hardened steels by heat treatment generates a phase contrast less than 5° even for hardness variations of 1 order of magnitude.[6] This suggests than a very small contrast signal should be expected from shot peened samples.

In Fig. 9 the Q signals corresponding to various τ_1 pulse widths and fixed τ_2 are reported as functions of the normalized pulse separation for the N7 sample and for two different modulation frequencies (500 Hz and 5 kHz). Figure 10 shows the shift of the zero position due to thermal response changes for both samples C5 and N7 at 500 Hz. The results are compared to that from the reference Zr sample. The ex-
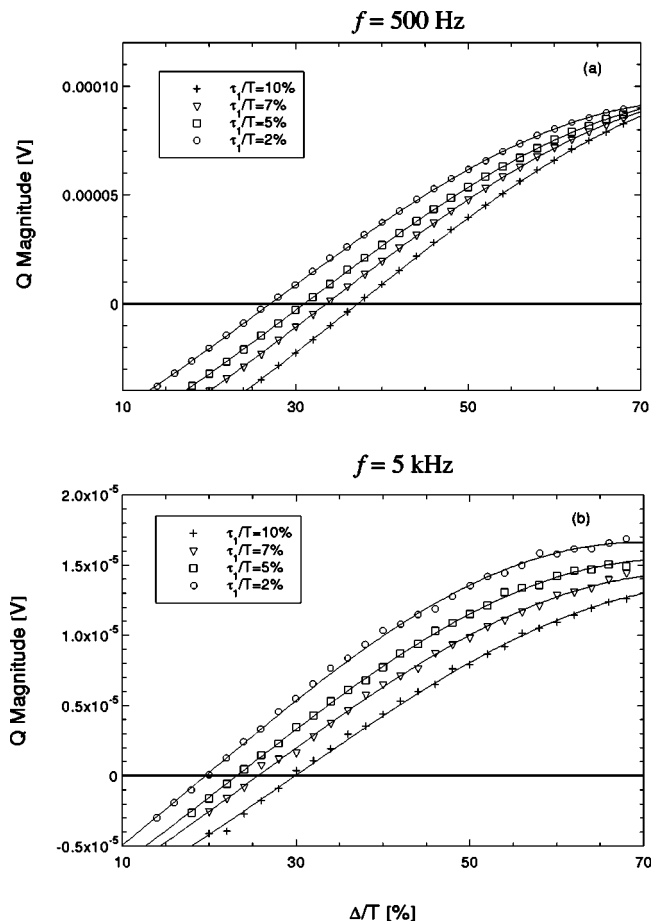

FIG. 9. Experimental Q component data obtained from the N7 sample for the τ_1/T values reported in the inset, and $\tau_2/T = 25\%$: (a) $f = 500$ Hz; (b) $f = 5$ kHz.

cellent agreement between theory and experimental results is confirmed: By fitting the data to Eq. (2), with the d value determined for the Zr sample obtained from the last row of Table I, we were able to precisely determine the Q component zero-crossing positions $\Delta_{0,Q}$. The $\tan[([(\Delta_{0,Q}+d)\pi/T]$ values shown in Fig. 11 were compared to the theoretical interpolations given by Eq. (4), in order to calcu-
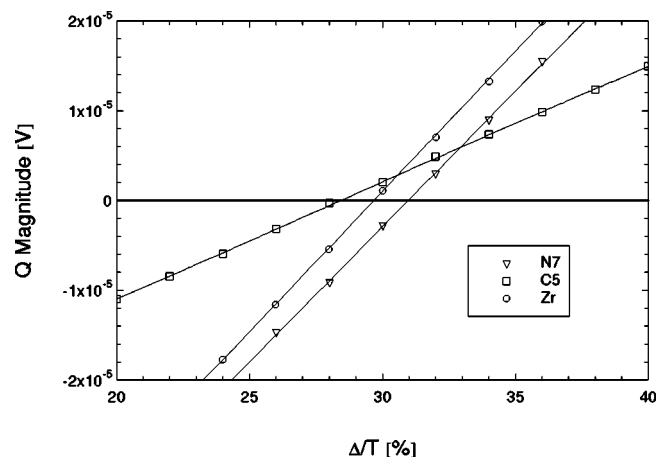

FIG. 10. The near-zero crossing region for the Q components of the two shot peened Zr–2.5Nb samples and the Zr reference. $\tau_1/T = 5\%$, $\tau_2/T = 25\%$, and $f = 500$ Hz.
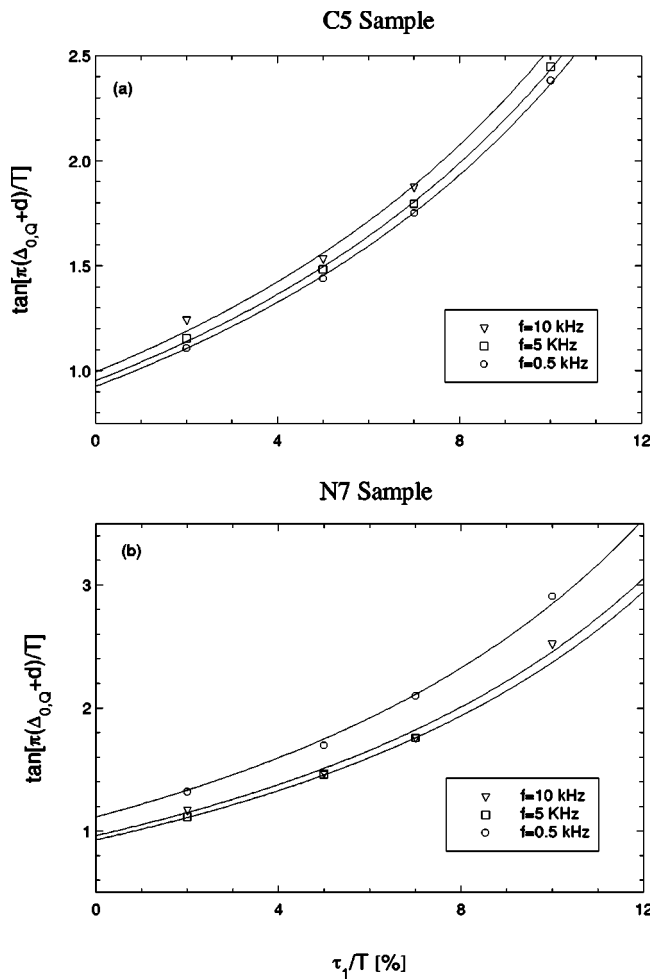
FIG. 11. Experimental Q component zero-crossing data obtained on the: (a) C5 and (b) N7 shot peened Zr–2.5Nb alloy samples for the modulation frequencies reported in the inset. The τ_1/T and τ_2/T values are the same as in Fig. 10.
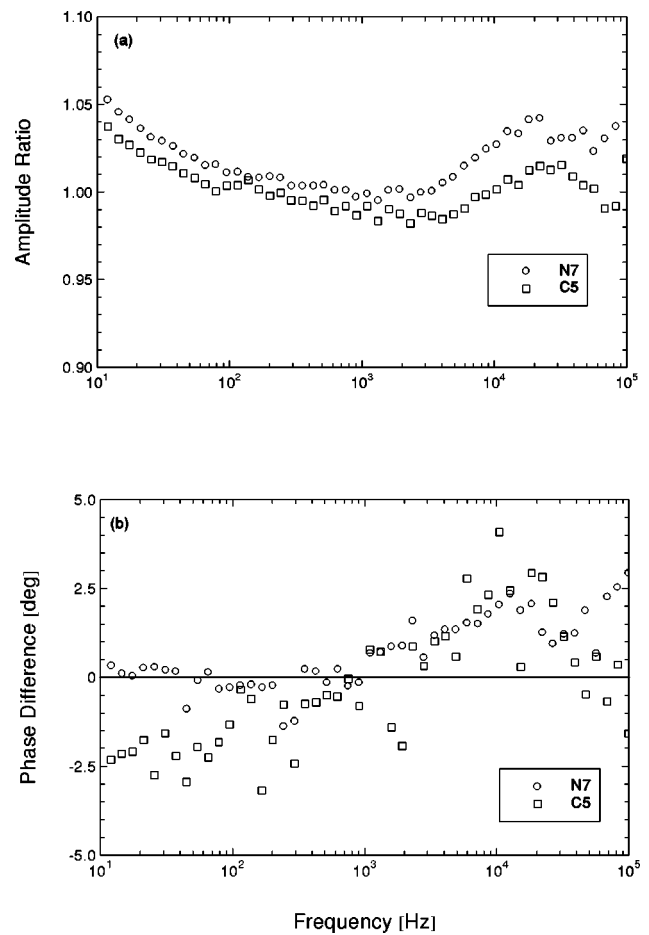

FIG. 12. Measured photothermal amplitude ratio: (a) and phase difference (b) for the two shot peened Zr–2.5Nb alloy samples. To aid the eye, the C5 ratio has been shifted upward by +0.5. The relative amplitudes are consistent with the slopes of the N7 and C5 curves in Fig. 10, which reveal a low photothermal amplitude response for the C5 sample.

late the $\mathrm{Im}[S(f)]/\mathrm{Re}[S(f)]$ values which are reported in Table II. The $\mathrm{Im}[S(f)]/\mathrm{Re}[S(f)]$ values obtained for the C5 sample reveal a trend as a function of the modulation frequency, which is quite consistent with the hardness profile. A shift from the homogenous sample response is expected when the thermal-wave diffusion length is on the order of the depth, where the hardness profile shows significant variations. Considering that the nominal thermal diffusivity value of the Zr–2.5Nb alloy is 0.093 cm^2/s,[7] at 0.5 kHz the thermal diffusion length is on the order of 75 μm, i.e., commensurate with the hardness depth. Therefore, the $\mathrm{Im}[S(f)]/\mathrm{Re}[S(f)]$ value at $f = 0.5$ kHz is higher than -1 expected from a semi-infinite homogeneous solid or, equivalently, the phase lag is less than $-45°$ ($-42.8°$). This is consistent with the fact that the hardened layer has an effective thermal diffusivity lower than that of the bulk.[3] At higher modulation frequencies, 5 and 10 kHz, the thermal diffusion length becomes ~ 20 μm. The corresponding hardness profile does not show large variations over this distance. This means that the sample can be assumed homogeneous over this depth and, accordingly, the $\mathrm{Im}[S(f)])]/\mathrm{Re}[S(f)]$ ratio assumes values roughly corresponding to $-45°$. On the contrary, the $\mathrm{Im}[S(f)]/\mathrm{Re}[S(f)]$ data obtained for the N7 sample do not

reveal any measurable trend with modulation frequency, reflecting the corresponding flat hardness profile behavior.

Conventional PTR frequency scans were further performed for comparison by using the same setup and the same 250 mW optical power for all the measurements. The only change was in the excitation-laser-beam modulation wave form, a 50% duty-cycle square wave. The experimental data, normalized by the data obtained from the Zr reference, are reported in Fig. 12. The systematic high-frequency-amplitude differences of the two curves in Fig. 12(a) are not meaningful, as extensive satellite PTR experiments with these and different Almen-intensity shot peened Zr–2.5Nb samples have shown that there exists no consistent trend of the signal with degree of hardening. Furthermore, unlike the $\mathrm{Im}[S(f)])]/\mathrm{Re}[S(f)]$ ratios of Table II, the presence of a hardness depth profile in the C5 sample (Fig. 8) cannot be measured from the similar amplitude trends of both samples throughout the entire frequency range in Fig. 12(a). The N7 $>$ C5 amplitude ratio in Fig. 12(a) is, however, consistent with the lower slope of the C5 curve in Fig. 10, which indicates a lower-amplitude thermal-wave signal at 500 Hz for the C5 shot peened Zr–2.5Nb alloy. The phase channel, Fig. 12(b), also clearly shows insensitivity to the differences in

hardness between the two shot-peened samples. Doubtless, any such differences are masked by the large data scatter in this figure.

In conclusion, the PTR experimental calibration of the novel common-mode rejection demodulation technique was shown to be a very promising high-detectivity measurement method for low-dynamic-range and poor-SNR signals, such as those obtained with thermal-wave diagnostics. Results with two shot peened Zr–2.5Nb samples have shown that this technique is sensitive enough to resolve minute differences in thermophysical properties resulting from mechanical structure changes of these materials after shot peening and to monitor hardness depth profiles by means of the value of the $\text{Im}[S(f)])]/\text{Re}[S(f)]$ ratio at several frequencies. Conventional single-ended frequency-scanned PTR detection proved unable to resolve these differences.[8]

ACKNOWLEDGMENTS

[1] A. Mandelis, S. Paoloni, and L. Nicolaides, Rev. Sci. Instrum. **71**, 2440 (2000).

[2] R. E. Imhof, B. Zhang, and D. J. S. Birch, in *Progress in Photothermal and Photoacoustic Science and Technology*, Vol. II: Non-Destructive Evaluation, edited by A. Mandelis (Prentice Hall, Englewood Cliffs, NJ, 1994), Chap. 7, pp. 186–236.

[3] See, for example, G. Busse and H. G. Walther, in *Progress in Photothermal and Photoacoustic Science and Technology*, Vol. I: Principles and Perspectives of Photothermal and Photoacoustic Phenomena, edited by A. Mandelis (Elsevier, New York, 1992), Chap. 5, pp. 207–298.

[4] *Surface Engineering*, edited by S. A. Meguid (Elsevier Applied Science, New York, 1990).

[5] K. F. Amouzouvi, L. J. Clegg, R. C. Styles, and J. E. Winegar (private communication).

[6] T. T. N. Lan and H. G. Walther, J. Appl. Phys. **80**, 5289 (1996).

[7] *ASM Handbook*, 10th ed., edited by Joseph E. Davis *et al.* (ASM International, Materials Park, OH, 1992), Vol. II, p. 666.

[8] M. Munidasa, T.-C. Ma, A. Mandelis, S. K. Brown, and L. Mannik, J. Mater. Sci. Eng. A **159**, 111 (1992).